

Fine Structure of the Hydrogen Atom. V* †

SOL TRIEBWASSER, ‡ EDWARD S. DAYHOFF, § AND WILLIS E. LAMB, JR. ||

Radiation Laboratory, Columbia University, New York, New York

(Received September 15, 1952)

Improvements in apparatus and techniques of measurement of the $2^2S_{1/2}-2^2P_{1/2}$ level shifts in hydrogen and deuterium are described. The more accurate results are $\mathcal{S}_H=1057.77\pm 0.10$ Mc/sec and $\mathcal{S}_D=1059.00\pm 0.10$ Mc/sec. These values are compared with results of quantum electrodynamic calculations.

The shape of the resonance curves has been examined in great detail and compared with theory. Assuming the theoretical value of the radiative width and hyperfine splittings, excellent agreement is obtained. Further, if only the radiative width is assumed, measurements on hydrogen reported here confirm theoretical hyperfine splittings to within 0.28 Mc/sec. Since contributions of the hyperfine structure of the $2S$ level have been measured to far greater accuracy, these results constitute a confirmation of the $2P$ hyperfine splittings to an accuracy of 1.0 percent.

INTRODUCTION

THIS is the fifth¹¹⁴ paper of a series reporting on measurements¹¹⁵ of the transition frequencies between the S and P states of the $n=2$ level of hydrogen and deuterium. The transitions with which we are concerned, from which the $2^2S_{1/2}-2^2P_{1/2}$ level shift \mathcal{S} is found, are shown in Fig. 57.

It was estimated from the average deviations of the mean of individual runs reported in Part IV that, aside from possible uncertainties of theoretical corrections, the center of any resonance being observed could be measured to a precision of 1 part in 1000 of the line width. On the other hand, the disagreement among the various runs was well outside¹¹⁶ of this accuracy. Due to the necessity of time consuming calculations of various corrections in Parts III and IV in order to evaluate \mathcal{S} from the recorded data, a considerable amount of data had been accumulated before this situation became apparent.

Our initial efforts to resolve the discrepancy between internal and external consistency were directed toward a modification of the apparatus and the experimental

procedure which would permit the elimination of some of the lengthy, and at times uncertain, corrections which previously were applied to the data. In addition, the problem of magnetic field calibration was examined for possible systematic or excessive random error.

R. MODIFICATIONS IN APPARATUS AND PROCEDURE

85. Rf Power and Frequency Stabilization

In the original technique for taking a run, the oscillator producing the transitions was allowed to drift slowly both in power and frequency, readings on both being taken at reasonable intervals. Corrections for these were applied to the data at some later time. For the present work a frequency regulator was developed¹¹⁷ which kept the frequency within 5 kc/sec of the nominal value throughout the run. The power drift problem was solved simply by using a finely controlled attenuator of conventional design which was varied manually so as to keep constant the power monitor crystal current. Slow drifts in crystal calibration were observed but did not introduce any error as they were small and fairly uniform.

86. Elimination of "Soft" β -Component

The $\alpha\epsilon$ resonance was measured at a midfield of about 1159 gauss. This was sufficiently near to the $\beta\epsilon$ crossing point (about 574 gauss) so that only a small percentage of the metastable atoms reaching the detector were in the β -state. Corrections discussed in Part IV, Sec. 73, were applied for residual β -state atoms. It was desired to eliminate this correction by removing even this small fraction of unwanted atoms. A small electric field in the proper direction was sufficient to quench the β -state atoms since the βf crossing point is very close (about 1190 gauss). As shown in Table VI of Part III, the electric field required lies in the z direction (π -polarization). To obtain this, a pair of plane electrodes was added between the bombarder and the rf interaction region.¹¹⁸ All $\alpha\epsilon$ data were taken

* Work supported jointly by the Signal Corps and ONR.

† Submitted by Sol Triebwasser in partial fulfillment of requirements for the degree of Doctor of Philosophy in the Faculty of Pure Science, Columbia University.

‡ Present address: Watson Scientific Computing Laboratory, Columbia University, New York, New York.

§ Present address: National Bureau of Standards, Central Radio Propagation Laboratory, Microwave Standards Section, Washington, D. C.

|| Present address: Department of Physics, Stanford University, Stanford, California.

¹¹⁴ Paper I, Phys. Rev. **79**, 549 (1950); Paper II, Phys. Rev. **81**, 222 (1951); Paper III, Phys. Rev. **85**, 259 (1952); Paper IV, Phys. Rev. **86**, 1014 (1952). Frequent references to these papers are made. Chapters, sections, figures, equations, tables, appendices, and footnotes of Part V are numbered consecutively after those of I-IV. The designation of states by letters $\alpha, \beta, a, b, c, d, e, f$ is explained in Fig. 14 of Part I, partially reproduced in Fig. 57 for convenience.

¹¹⁵ Earlier results were reported as follows: $\mathcal{S}=1000\pm 100$ Mc/sec, W. E. Lamb, Jr., and R. C. Retherford, Phys. Rev. **72**, 241 (1947); $\mathcal{S}=1062\pm 5$ Mc/sec, Phys. Rev. **75**, 1325 (1949); $\mathcal{S}_H=1058.27\pm 1.0$ Mc/sec, $\mathcal{S}_D=1059.71\pm 1.0$ Mc/sec in Part IV, Phys. Rev. **86**, 1014 (1952). Part II describes the apparatus used in the measurements reported here.

¹¹⁶ See Table XVI, Part IV.

¹¹⁷ E. S. Dayhoff, Rev. Sci. Instr. **22**, 1025 (1951).

¹¹⁸ See Fig. 27, Part II.

in the presence of this "low voltage quenching" field. As described in Sec. 73 of Part IV, by measuring the quenching produced by these additional electrodes as a function of the applied field one can calculate the field required to quench adequately the "soft" β -component of the metastable beam. The electric field used in all of the αe runs taken was 4.6 volts/cm.

87. Rf Lines

The αf transition required an rf electric field with polarization perpendicular to the magnetic field. The earlier measurements were taken with a transmission line whose electric polarization was predominantly π , with σ -fields obtained only from the fringing of the field. In addition, the αf transition could not be taken at a sufficient separation in field from the αe peak to avoid overlap from that transition. The result was a line shape complicated by magnetic field inhomogeneity and relatively uncertain overlap. The measurements reported here were taken with transmission lines whose predominant polarizations were the desired ones for each of the transitions: σ for αf , π for αe .

The σ -polarization line is actually a modified coaxial cavity resonator in which the center conductor does not quite extend to the end plate, thereby leaving a gap through which the metastable atoms can pass. This arrangement is shown in Fig. 58. The cavity resonator is entirely inside the vacuum envelope and tuning is accomplished from the outside by means of an "O-Ring" sliding joint. The resonator part of the structure is entirely gold-plated to simplify the cleaning of surfaces exposed to the beam. This resonator has

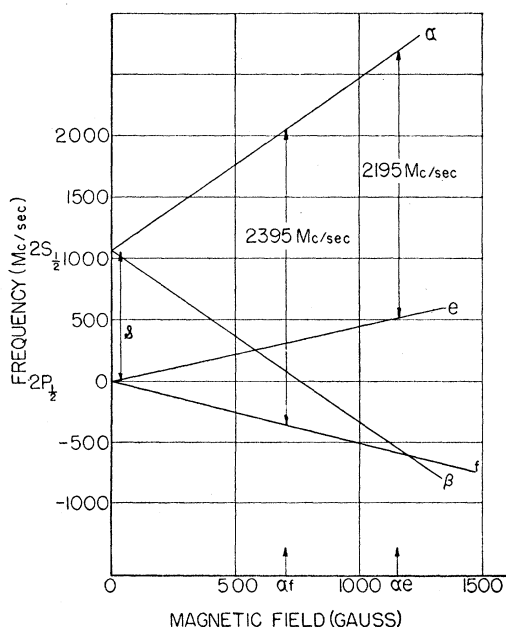


FIG. 57. Energy levels as a function of magnetic field for the $2^2S_{1/2}$ and $2^2P_{1/2}$ levels of hydrogen and deuterium. The letter designation of the states is as Fig. 14 of Part I.

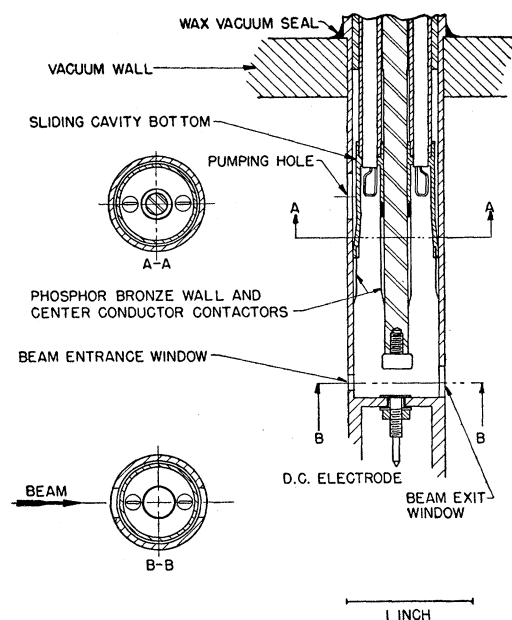


FIG. 58. Rf line used for the observation of σ -transitions. The static magnetic field is perpendicular to the plane of the drawing, while the beam of metastable atoms passes from left to right in the plane of the drawing.

a relatively high Q factor over the range from 1600 Mc/sec to 11,000 Mc/sec and consequently requires very little excitation power. The reduced power requirement in turn proved to be a major advantage at the higher frequencies where the other rf lines that had been constructed for this experiment were very inefficient. All of the αf data reported in this paper as well as the αa and αc data to be reported in Part VI were taken with this line.

The rf electric field of this line has a high degree of symmetry, possessing only the σ -components at all points along the center line of the beam. Atoms near the sides of the beam experience a small π -field component. From observations of the relative strengths of the αe and αf transitions at 1615 Mc/sec, it is estimated that the effective ratio of σ to π intensities is 10 to 1.

The π -polarization line shown in Fig. 59 was used for the αe measurements reported here. It differs only in detail from the line used for all measurements reported in Part IV. The rf and dc plates are equal in size and symmetrically placed about the axis of the rf line. The dc plate is provided with a solid metal back which is separated from the wall of the rf line by a 2-mil thick Teflon strip which has sufficient capacitance to act as a return path to ground for the rf current. The line is terminated below the interaction region in a crystal load whose current is used to monitor the rf power.

88. Magnetic Field Measurement

Descriptions of the magnet, the magnet current regulator and the method of magnetic field measure-

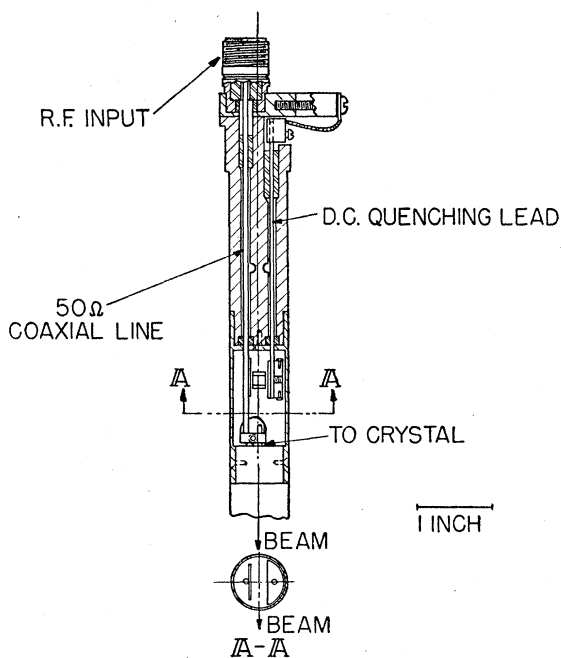


FIG. 59. Rf line used for the observation of π -transitions. The static magnetic field is horizontal in the plane of the drawing. The beam of metastable atoms is perpendicular to the plane of the drawing.

ment were given in Secs. 36, 38, and 39 of Part II. Briefly, the magnetic field is computed from Eq. 96a:

$$H = (\text{constant}) \times R, \quad (96a)$$

where R is the setting of an appropriate resistance box and the constant is measured at some known magnetic field. Improvements in the measurement of this magnetic field calibration constant are given in Sec. 100 of Part VI.¹¹⁹

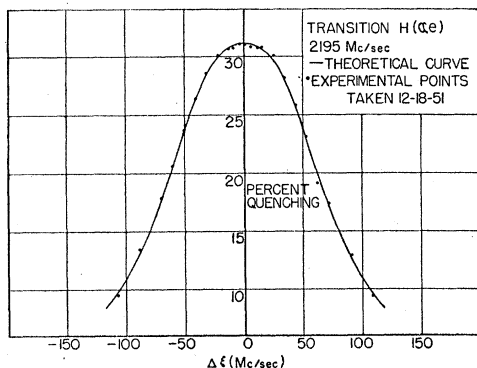


FIG. 60. $H(\alpha e)$ panoramic at 2195 Mc/sec, $H_0 = 1159.5$ gauss. Data are taken as a function of magnetic field H but plotted for convenience against a frequency variable ξ , using the conversion $(d\xi/dH) = 1.0204$ Mc sec⁻¹ gauss⁻¹.

¹¹⁹ Dayhoff, Triebwasser, and Lamb, Phys. Rev. **89**, 106 (1953).

S. LINE SHAPE

89. Panoramics

The measurement of the center of a line to 0.1 percent of its width requires a careful study of the line shape and any possible asymmetries. The gross verification of the theory is achieved by plotting quenching as a function of magnetic field. Figures 60 to 63 show such curves except that the abscissa is plotted as "Mc/sec away from resonance" ξ . The effect of Zeeman curvature is too small to be seen on this scale, and the use of ξ as the abscissa is for convenience only. The solid line is a plot of

$$\varphi = \frac{\sum_m \int_0^\infty (1 - e^{-\psi_m/y}) \exp(-y^2) y^2 dy}{\sum_m \int_0^\infty \exp(-y^2) y^2 dy} \times 100, \quad (255)$$

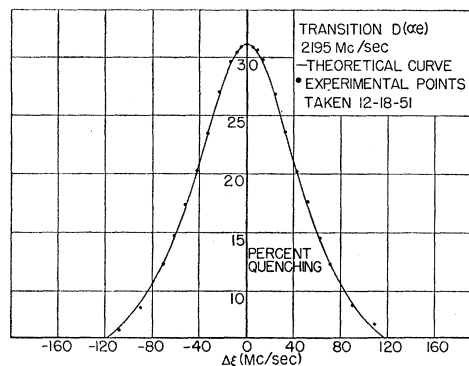


FIG. 61. $D(\alpha e)$ panoramic at 2195 Mc/sec, $H_0 = 1159.6$ gauss. Data are taken as a function of magnetic field H but plotted for convenience against a frequency variable ξ , using the conversion $(d\xi/dH) = 1.0207$ Mc sec⁻¹ gauss⁻¹.

where

$$\psi_m = Ab^2 / [(\xi - a_m)^2 + b^2]. \quad (256)$$

The only difference between (255), (256), and (197), (199) of Part III is the assumption of a $y^2 \exp(-y^2)$ distribution of metastable atoms rather than $y^3 \exp(-y^2)$. We again assume a $v^3 \exp(-v^2/U^2)$ distribution for atoms emerging from the hot tungsten oven,¹²⁰ but a $1/v$ dependence of the interaction time of the atoms with electrons in the bombarder¹²⁰ reduces the exponent of the velocity to 2. The parameter A is a measure of the effective rf power, b the theoretical lifetime of the $2P$ states, a_m the frequency displacement due to hyperfine structure of the component with $m_I = m$, ξ the number of Mc/sec away from the center of the composite resonance, and y is the dimensionless velocity variable, $v/(2kT/M)^{1/2}$. The simple velocity distribution assumed is, in fact, modified by motional Stark quenching¹²¹

¹²⁰ See Figs. 28 and 29, Part II.

¹²¹ See appendices II and III, Part I.

and recoil in the bombarder.¹²¹ Measurements described in Appendix VII do, however, indicate that $y^2 \exp(-y^2)$ is a good approximation to the actual velocity dependence of the distribution of metastable atoms leaving the bombarder.

The αf data were taken by starting on one side of the resonant magnetic field and moving in steps indicated by the experimental points until a curve was completed. The αe curve, on the other hand, was taken by starting at the peak of the resonance and taking points alternately on the two sides of the curve. The latter method eliminates asymmetry in the experimental points due to drift of power monitor calibration. The $H(\alpha f)$ panoramic shows a slight asymmetry in the peaks which is probably due to just this effect. Theoretical asymmetries discussed in Sec. 92 are too small to show up on the scale of this plot.

90. Line Widths

The line width may be subjected to a more careful check than the over-all shape because of the large

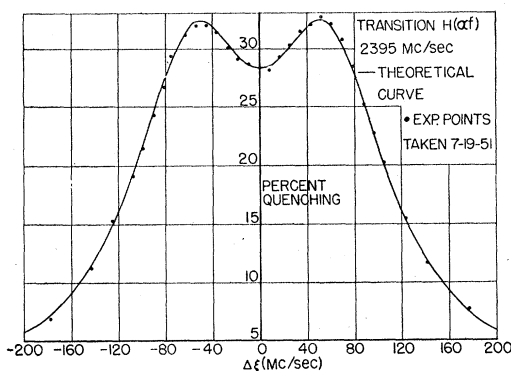


FIG. 62. $H(\alpha f)$ panoramic at 2395 Mc/sec, $H_0=703.77$ gauss. Data are taken as a function of magnetic field H but plotted for convenience against a frequency variable ξ , using the conversion $(d\xi/dH)=1.9216$ Mc sec⁻¹ gauss⁻¹.

amount of data accumulated at the working points. The procedure used consists of comparing the fractional quenching at the working points with that predicted theoretically.

The method of taking data outlined in Sec. 45 of Part II was followed. Details are given in Sec. 75 of Part IV. To recall the technique: A nominal resonant magnetic field H_0 was chosen on the basis of information from previous runs to be as near the true resonant magnetic field as possible. Then "working points" were selected above and below the resonant field to fall about at the points of inflection of the panoramic. The usual run consisted of 9 lines of data, 4 at one of the working points and 5 at the other, and two lines at H_0 . The rf power was set for a previously selected peak quenching [31 percent for $D(\alpha f)$, $H(\alpha e)$, $D(\alpha e)$; 28.3 percent for $H(\alpha f)$] at H_0 . The measurements at H_0 were taken at the beginning and end of a run. A line of data at one of the working points consisted of three

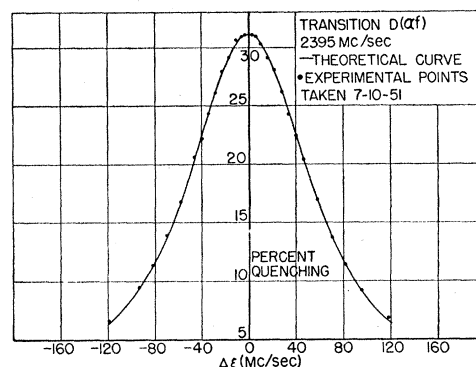


FIG. 63. $D(\alpha f)$ panoramic at 2395 Mc/sec, $H_0=704.57$ gauss. Data is taken as a function of magnetic field H but plotted for convenience against a frequency variable ξ , using the conversion $(d\xi/dH)=1.9257$ Mc sec⁻¹ gauss⁻¹.

measurements of the total beam size as measured by dc quenching of all the metastable α state atoms alternated with four measurements of the rf quenching for the previously set power and frequency. This procedure compensates for a uniform drift of galvanometer and intensity of the metastable beam as discussed in Sec. 75 of Part IV.

Table XVII shows percent rf quenching at the working points for all runs. Each result was reduced to the nominal peak quenching as follows: Quenching at the

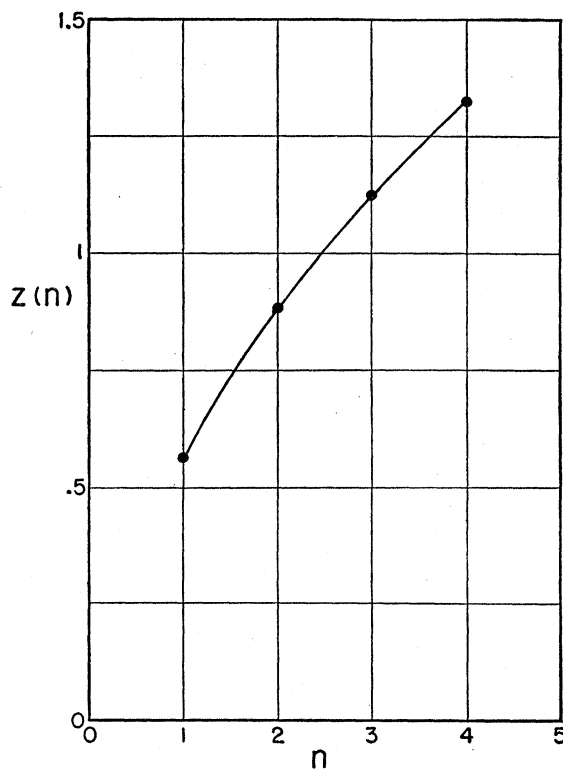


FIG. 64. $\Theta(n) = \left[\int_0^\infty \exp(-y^2) y^n dy \right] / \left[\int_0^\infty \exp(-y^2) y^{n-1} dy \right]$ plotted as a function of the velocity distribution index n .

TABLE XVII. Width data: Measured widths for all runs taken. Quenching is normalized to 31 percent at peak for $H(\alpha e)$, $D(\alpha e)$, $D(\alpha f)$, and 28.3 percent for $H(\alpha f)$ using measured quenching at peak associated with each run. Theoretical values are given for same peak quenching and actual operating points.

Runs $H(\alpha e)$		Runs $D(\alpha e)$	
Date	Percent quenching at working points	Date	Percent quenching at working points
11/30/51	20.407	11/16/51	20.654
12/ 3/51	20.218	11/19/51	20.776
12/ 7/51	20.162	11/29/51	20.906
12/13/51	20.131	12/13/51	20.648
12/15/51	20.141	12/14/51	20.633
Average	20.212	Average	20.723
Av. dev.	0.085	Av. dev.	0.094
Theoretical for $\Delta H = \pm 60.054$ gauss	20.286	Theoretical for $\Delta H = \pm 40.040$ gauss	20.805

$H(\alpha f)$		$D(\alpha f)$	
Date	Percent quenching at working points	Date	Percent quenching at working points
9/25/51	21.644	9/25/51	20.781
9/28/51	21.344	9/28/51	20.661
10/ 2/51	21.614	10/ 2/51	20.774
10/ 3/51	21.264	10/ 3/51	20.640
10/ 4/51	21.629		
Average	21.486	Average	20.714
Av. dev.	0.091	Av. dev.	0.064
Theoretical for $\Delta H = \pm 52.001$ gauss	21.497	Theoretical for $\Delta H = \pm 23.386$ gauss	20.734

working points and the peak of the curve was calculated for two slightly different values of A [Eq. (256)] and $(\Delta\phi \text{ operating point})/(\Delta\phi \text{ peak})$ evaluated. From the average percent quenching at the peaks, one can evaluate a correction to reduce the run to the nominal peak quenching for the particular transition. Since the peak quenching was set fairly carefully before the actual run data were taken, this never represented a correction of more than 0.5 percent in ϕ . Theoretical values were obtained from Eq. (255) modified as in Eq. (258) for motional Stark quenching and are seen to be consistent with the experimental values. The fact that the theoretical value is always higher may be an indication of the rf power narrowing discussed in Appendix IV of Part III.

If one assumes the theoretical value of the radiative width, the measurements summarized in Table XVII

TABLE XVIII. Slope measurement results (details explained in text, Sec. 91).

Transition	Date	Measured slope at working points $\Delta\phi/\Delta\xi$	Number of measurements	Theoretical slope at working points $\Delta\phi/\Delta\xi$
$H(\alpha e)$	12/13, 15/51	0.3000 ± 0.0084	4	0.3012
$D(\alpha e)$	12/13, 14/51	0.3348 ± 0.0018	4	0.3387
$H(\alpha f)$	7/31/51	0.3090 ± 0.0107	9	0.3023
$D(\alpha f)$	7/27/51	0.3271 ± 0.0086	9	0.3264

constitute a measurement of the a_m used in calculating the theoretical panoramics [Eqs. (255) and (256)]. The stated uncertainty in the observed "percent quenching at the working points" (0.085 percent in the case of the $H(\alpha e)$ transition) can be translated into an uncertainty in a_m . Following this scheme, we find that the results given for the $H(\alpha e)$ and $H(\alpha f)$ transitions confirm the hyperfine structure contributions to resonance width calculated from theoretical formulas given in Sec. 56 of Part III to within 0.20 Mc/sec in each case. Unpublished measurements of the sharp $H(\alpha\beta)$ transitions yield confirmation of the theoretical hyperfine structure of the $2S$ states to far greater accuracy, so we consider that the results being discussed here constitute a confirmation within 1.0 percent of the theoretical hyperfine structure splitting of the $2P$ states. The absolute accuracy of the deuterium measurements is at least as good as the hydrogen results. Hyperfine splittings in the former, however, are much smaller.

91. Slope at Operating Points

Since the exact resonant magnetic field H_0 was not known in advance, the runs did not have the fractional quenching exactly equal at the two working points. To arrive at this value, H_0 , one must know $d\phi/dH$ at the working points. This was calculated from the theoretical panoramic. In addition, measurements were made to verify the theoretical slopes. Table XVIII shows the results of these measurements. In the case of the αe transitions, two magnetic fields straddling a working point were chosen—in some cases 10 gauss apart and in others about 15 gauss apart. The rf power was set so as to give the correct quenching at the peak of the resonance. The galvanometer was then read as the magnetic field was alternated between the two values until a total of about 20 or 30 readings were taken. The average change in the galvanometer reading was computed. Then the measurements were repeated with rf power off to subtract any possible change in beam size with the relatively small change in magnetic field. At the beginning and end of this measurement the full size of the beam was measured by dc quenching. The average change in galvanometer reading with rf, minus the average without rf, divided by the total beam size, gave the change in fractional quenching. This procedure assumed only a small change in the beam size as the field was changed over the 10 or 15 gauss of the measurement, a condition satisfied with sufficient accuracy in the experiment. One could then calculate the slope of the quenching vs magnetic field curve. Each of the four measurements contributing to results in Table XVIII consisted of just such a measurement, two at each working point. Since the shift in the galvanometer reading was at most .6 cm, it was a difficult measurement to make with high precision. The small average deviation shown for $D(\alpha e)$ is probably accidental. Theoretical slopes were used in calculating the small corrections to the data of actual runs.

The αf slope was measured by selecting two magnetic field values straddling each of the original working points and taking alternate half-lines of data at these two points separated by about 6 gauss. These were taken on one day, 4 straddling one working point and 5 straddling the other. Again the measurements were in agreement with theoretical values. In none of the transitions was there any apparent asymmetry between the slopes at the two operating points. In all cases except the $D(\alpha e)$ transition, the measured slopes differ from the theoretical slopes by less than the average deviation.

T. RESULTS

92. Corrections Applied to Runs

The true resistances of the resistance boxes used in the magnetic field measurement, were found by correcting the nominal values of individual decades as measured against a precision resistor.¹²² These values were then corrected for the temperatures of the boxes and the values at the working points corrected in this way were averaged. The result is the nominal resonant magnetic field resistance. Corrections were then applied for the difference in percent quenching at the working points yielding the corrected resonant magnetic field resistance [Eq. (252), Part IV].

$$\bar{R} = \frac{1}{2}(R_a + R_b) + \frac{1}{2}(\varphi_b - \varphi_a)/(d\varphi/dR). \quad (252)$$

The calibration constant R/H was evaluated from the proton resonance data¹¹⁹ corrected for temperature coefficients of the resistance boxes and frequency of the secondary standard as compared with the 5 Mc/sec standard frequency broadcasts of the National Bureau of Standards. The beat frequency was measured every day on which a run was taken. Interpolation for the magnet temperature was used to find R/H for the average temperature of the magnet for the run. Then H for the run is given by $\bar{R}/(R/H)$. Since the frequency of the rf used for the transitions is an integral multiple of the nominal 5.0 Mc/sec secondary standard, an additional correction must be applied for the true frequency of the oscillator. The resonant magnetic fields so calculated are given in Table XIX. The average deviation given for each run was computed from the square root of the sum of the squares of the average deviations of φ_a and φ_b in the run multiplied by $\frac{1}{2}(dH/d\varphi)$. Weights applied to individual runs are taken as $N/(\text{Av. dev.})^2$, where N is the number of lines of data taken at the working points.

93. Asymmetry and Shift Corrections

The asymmetry and shift corrections are shown in Table XX which is similar to Table XV of Part IV except for the assumption of a $y^2 \exp(-y^2)$ velocity distribution and the inclusion of a correction for the

TABLE XIX. Summary of runs: H_0 is the measured field at the center of the resonance after all corrections, but asymmetry and shift corrections common to all runs of a single transition have been made.

H(αe)(2195 Mc/sec)				
Date	H_0 (gauss)	Av. dev. (gauss)	N	Relative weight
11/30/51	1159.490	0.511	11	42
12/ 3/51	1159.511	0.229	9	173
12/ 7/51	1159.727	0.232	11	204
12/13/51	1159.485	0.182	11	332
12/15/51	1159.361	0.314	11	112
Average	1159.532±0.093			
D(αe)(2195 Mc/sec)				
11/16/51	1159.397	0.245	9	150
11/19/51	1159.770	0.442	9	46
11/29/51	1159.486	0.223	9	181
12/13/51	1159.609	0.175	11	359
12/14/51	1159.584	0.160	9	352
Average	1159.555±0.073			
H(αf)(2395 Mc/sec)				
9/25/51	703.669	0.125	11	70
9/28/51	703.624	0.135	9	49
10/ 2/51	703.688	0.198	11	28
10/ 3/51	703.750	0.142	5	25
10/ 4/51	704.082	0.298	5	6
Average	703.685±0.046			
D(αf)(2395 Mc/sec)				
9/25/51	704.515	0.108	11	94
9/28/51	704.475	0.128	11	67
10/ 2/51	704.521	0.154	11	46
10/ 3/51	704.499	0.123	5	33
Average	704.503±0.017			

“low voltage quencher” asymmetry in the case of αe transitions. Improved rf electric field polarization reduced “overlap” and “forbidden components” corrections sufficiently so that they may be neglected.

The Stark effect correction was calculated using the general technique applied to the other asymmetries, rather than by the method outlined in Sec. 57 of Part III. The velocity dependence of the Stark shift was inserted explicitly into Eq. (255) by modifying Eq. (256) as follows:

$$\psi_m = Ab^2/[(\xi - a_m - a_s y^2)^2 + b^2], \quad (257)$$

where a_s is the Stark shift in Mc/sec for an atom traveling at the velocity for which $y=1$. This was

TABLE XX. Asymmetry and shift corrections: Corrections to g in Mc/sec calculated at the working points for peak quenching to which each transition is normalized.

Transition	H(αe)	D(αe)	H(αf)	D(αf)
Matrix element variation	-0.588	-0.366	-0.284	-0.125
Quenching asymmetry	-0.077	0.034	-0.133	0.012
Incomplete Back-Goudsmit effect and Zeeman curvature	-0.923	-0.105	-2.733	-0.195
Stark effect	0.308	0.150	-0.071	-0.033
Total correction	-1.280	-0.287	-3.221	-0.341
	Mc/sec	Mc/sec	Mc/sec	Mc/sec

¹²² Described in detail in reference 119, Sec. 98a.

TABLE XXI. Summary of results.

Transition	Frequency Mc/sec	\bar{H}_0 (gauss)	Av. dev. (gauss)	\mathcal{S} (Mc/sec)	Asymmetry and shift correc- tions	\mathcal{S} (Mc/sec) corrected	Av. dev. (Mc/sec)
H(αe)	2195	1159.532	0.093	1059.032	-1.280	1057.752	0.095
D(αe)	2195	1159.555	0.073	1059.344	-0.287	1059.057	0.074
H(αf)	2395	703.685	0.046	1061.016	-3.221	1057.795	0.089
D(αf)	2395	704.503	0.017	1059.291	-0.341	1058.950	0.033

$\mathcal{S}_H = 1057.77 \pm 0.10$ Mc/sec
 $\mathcal{S}_D = 1059.00 \pm 0.10$ Mc/sec

calculated as described in Sec. 57 of Part III, except that the required matrix elements were taken from the intermediate field wave functions at the resonant magnetic field at which the transition was observed. Stark corrections given in Table XV of Part IV were calculated for the limiting case of small rf quenching and for the zero field matrix elements. The result of the sample calculation given in Sec. 57 of Part III is twice as large as the equivalent result of Part IV due to the incorrect velocity distribution assumed in the earlier calculations.

The only other substantial difference between Table XIX and Table XV is in the Zeeman curvature correction for the αf transition, where an incorrect sign was used in Part IV for the curvature of the transition frequency with respect to magnetic field.

The quenching asymmetry introduced by the additional β -state quencher mentioned above is calculated by a modification of Eqs. (203), (204), Part III as follows:

$$\varphi = \frac{\sum_m \int_0^\infty e^{-\rho y} e^{-r/y} (1 - e^{-\psi m/y}) \exp(-y^2) y^2 dy}{\sum_m \int_0^\infty e^{-\rho y} e^{-r/y} \exp(-y^2) y^2 dy} \times 100, \quad (258)$$

where r is a measure of the decay rate of α -state atoms due to the additional electrodes computed from Eq. (42) of Part I. Only quenching due to αe coupling is taken into account. The parameter r is about $(\frac{1}{10}) \rho$ in the experiment, so that the effect of αb quenching will surely be negligible in so far as any asymmetry is concerned.

94. Results

Table XXI gives the results for each of the transitions. The average deviations quoted were computed directly from the column labeled " H_0 " in Table XIX, with weighting as given in the column labeled "Relative Weight" assigned to the deviations. The deviations in deuterium are smaller than those for hydrogen mostly due to the larger signal and reduced relative noise in the case of the heavier isotope. The smallness of the average deviation for the D(αf) is probably fortuitous. We consider that the average deviations for the hydrogen transitions and the D(αe) are representative of the ultimate accuracy inherent in the apparatus.

In estimating a limit of error, one must consider any residual systematic errors in the experimental technique and in the theoretical corrections applied to the results. Uncertainties of velocity distribution could lead at most to an additional correction of 0.02 Mc/sec. Due to the fact that the αf , αe Stark effects are opposite in sign, the average \mathcal{S} is affected less than either. The presence of unknown static electric fields would be a source of error, but it is felt that there are no residual effects of this kind near the stated accuracy in magnitude. An estimate of the effect of magnetic field inhomogeneity yields an error of less than 0.01 Mc/sec in the worst possible case.

From Table XXI, taking the average of αe and αf results for each of the isotopes considered, one arrives at $\mathcal{S}_H = 1057.77$ Mc/sec for hydrogen and $\mathcal{S}_D = 1059.00$ Mc/sec for deuterium with an accuracy of ± 0.10 Mc/sec for each. Weighted means are not used because it is felt that αe and αf measurements have equal inherent accuracies, fluctuations in the individual deviations being of a normal random nature. The precision stated is arrived at as follows: The average deviation of the mean for any individual run is of the order 0.10 Mc/sec. Then the average deviation of the mean for an individual transition would be 0.10 divided by $\sqrt{4}$ or $\sqrt{5}$ as the case may be for the number of runs in a transition, or about 0.05 Mc/sec. Finally, dividing 0.05 by $\sqrt{2}$ to take into account the two independent measurements represented by the αe and αf transitions, would yield the average deviation of the results stated. The accuracy given (0.10 Mc/sec) is, then, approximately $3 \times$ (average deviation of the mean).

It is worth noting that the magnitudes of average deviations as one progresses from "individual runs" to "average for a transition" to "average of different transitions," present a picture consistent with that to be expected from statistical theory. One would infer that the fluctuations in the measurements are probably random in nature.

V. EVALUATION

95. Comparison of Results with Theory

The present status of theoretical calculations of the level shift has been summarized in an accompanying paper by Salpeter.¹²³ He finds, apart from some specific contributions as yet uncalculated,

$$\begin{aligned} \mathcal{S}_H &= (1057.19 \pm 0.16) \text{ Mc/sec;} \\ \mathcal{S}_D &= (1058.49 \pm 0.16) \text{ Mc/sec.} \end{aligned}$$

These calculated values are about 0.5 Mc/sec smaller than the equivalent experimental results, although the $(\mathcal{S}_D - \mathcal{S}_H)$ values are in excellent agreement. This discrepancy between theoretical and experimental level

¹²³ E. E. Salpeter, Phys. Rev. **89**, 92 (1953). See also Sec. 84 of Part IV. The authors are indebted to Dr. Salpeter for the communication of his unpublished results.

shifts is well outside the estimated error and is as yet unresolved.

The authors have benefited greatly from many valuable discussions of the theoretical aspects of this work with Professor N. M. Kroll. We wish to thank Messrs. J. Heberle and H. Reich and other members of the Columbia Radiation Laboratory staff for cooperation and assistance in the experimental work, and Messrs. A. H. Barrett and R. Herman for assistance in the computations.

APPENDIX VII. VELOCITY MEASUREMENTS

The motional electric field $\mathbf{E} = (\mathbf{v}/c) \times \mathbf{H}$ provides a means for measuring a suitably defined average velocity of metastable atoms in the beam since it produces a Stark quenching of the beam.¹²⁴ The measured average velocity can then be used as a verification of the velocity distribution assumed in the calculations of the various corrections. The measurement consists of applying to the atoms a uniform adjustable electric field along the direction of the motional field. The quenching of the beam by the resulting electric field will be at a minimum when the applied field neutralizes on the average the motional field for the beam.

For the purposes of this analysis, a satisfactory approximation may be obtained by starting with the assumption that the metastable atoms in the beam are distributed in velocity according to the law

$$f(v, n) = N \exp(-y^2)y^n, \quad (259)$$

where y is the previously defined dimensionless velocity variable, and N is a normalizing constant. The free parameter n is used to allow roughly for distortions of the distribution due to such causes as recoil, preferential scattering of slow atoms, motional Stark quenching of the faster atoms elsewhere in the beam, and the possible velocity dependence of the efficiency of the metastable atom detector. Excluding these effects, one would expect n to be 2 (Sec. 89).

The fractional quenching can be written as

$$\varphi = Z(E, n)/Z(\infty, n), \quad (260)$$

where the quenching function Z is given by

$$Z(E, n) = \int_0^\infty \left[1 - \exp\left\{ \frac{-a[E - (U/c)Hy]^2}{y} \right\} \right] \times \exp(-y^2)y^n dy. \quad (261)$$

The coefficient a is a constant for a fixed magnetic field, E is the applied electric field, U is $(2kT/M)^{1/2}$ and y is v/U . In the region of small quenching, the exponential function above can be expanded and the first nonzero

term of Z retained. Z (and φ) will be a minimum when

$$\begin{aligned} dZ/dE &= d/dE \int_0^\infty a \left[E - \left(\frac{UH}{c} \right) y \right]^2 \exp(-y^2)y^{n-1} dy \\ &= 2a \left[E \int_0^\infty \exp(-y^2)y^{n-1} dy \right. \\ &\quad \left. - \frac{UH}{c} \int_0^\infty \exp(-y^2)y^n dy \right] = 0; \end{aligned}$$

or, the value of E which leads to minimum quenching is given by

$$E_{\min} = (U/c)H\Theta(n), \quad (262a)$$

$$\Theta(n) = \left(\int_0^\infty \exp(-y^2)y^n dy \right) / \left(\int_0^\infty \exp(-y^2)y^{n-1} dy \right). \quad (262b)$$

The function $\Theta(n)$ is plotted as a function of n in Fig. 64. Measured values of $E_{\min}/[(U/c)H]$ are given in Table XXII together with the graphically found value of n which would lead to the observed Θ . The measurement is made by substituting for the rf interaction region two round plates, 0.620 inches in diameter, 0.190 inches apart, parallel to and symmetrically placed about the plane determined by the magnetic field and the direction of the beam of atoms. To eliminate the effect of contact potentials, minima of φ as a function of E are taken for both polarities of the magnetic field. In the one case we observe $E+E_c$ and in the other, $E-E_c$; the average of the two observations eliminates E_c .

The theory given above assumes perfect uniformity of electric field in the interaction space. Fringing of this field will lead to an apparent value of the index n which is too high. The error to be expected for the actual geometry of the experiment has been estimated to be large enough to account for the observed deviation of n from 2.

The apparent decrease of n when the magnetic field is increased is interpreted as evidence for preferential

TABLE XXII. Observed velocity distribution indices for various magnetic fields.

Magnetic field (gauss)	$\Theta(n)$	n
Deuterium		
575	1.007	2.5
705	0.945	2.2
1140	0.944	2.2
3670	0.793	1.7
Hydrogen		
575	1.028	2.6
1140	0.994	2.4

¹²⁴ See Part I, Appendix II.

quenching by the motional electric field of the faster atoms before they enter the interaction space. Aside from the relatively slow variation with magnetic field of the denominator of the formula for the life time¹²⁵ of the α -state, this type of quenching varies directly with H^2 .

Although this technique for measurement of n does

¹²⁵ See Part I, Eq. (42).

not give much accuracy, the results may be taken to provide some confirmation of the assumed velocity distribution. Fortunately, as previously discussed (Sec. 93), the only correction sensitive to the value of n is that due to motional Stark effect. Uncertainty in this has been estimated at 10 percent of the correction itself and has been included in the estimate of error of the results.

Fine Structure of the Hydrogen Atom. VI*†

EDWARD S. DAYHOFF,‡ SOL TRIEBWASSER,§ AND WILLIS E. LAMB, JR.¶
Radiation Laboratory, Columbia University, New York, New York

(Received September 15, 1952)

Measurements of improved accuracy of transition frequencies from the $2^2S_{1/2}(m=+\frac{1}{2})$ state to several of the $2^2P_{3/2}$ magnetic sub-states in deuterium are presented and analyzed. The shape of the observed resonance curves is discussed and compared with theory.

The experimental result is given for the $2^2P_{3/2}-2^2S_{1/2}$ separation, $\Delta E_D - \delta_D = 9912.59 \pm 0.10$ Mc/sec, for deuterium. This is combined with the result for δ_D from the preceding article to obtain the $2^2P_{3/2}-2^2P_{1/2}$ separation, $\Delta E_D = 10,971.59 \pm 0.20$ Mc/sec for deuterium. From ΔE_D and the auxiliary constants R_D and c a new value is computed for the fine structure constant $\alpha = 1/(137.0365 \pm 0.0012)$. The uncertainty stated is considered to be a limit of error for our experimental procedure without allowance for the uncertainty of the auxiliary constants.

INTRODUCTION

THE preceding articles of this series¹²⁸ have discussed the theory of measurement of the fine structure of hydrogen and have presented highly accurate results for the $2^2S_{1/2}-2^2P_{3/2}$ shift δ for hydrogen and deuterium. On the basis of the foundation already laid, measurements of improved accuracy of transition frequencies from the $2^2S_{1/2}(m=+\frac{1}{2})$ state to several of the $2^2P_{3/2}$ magnetic sub-states in deuterium are here discussed. The improved accuracy results mainly from improved magnetic field measurement technique, the elimination of some experimental corrections, and better stability of the equipment. The splitting of the levels in a magnetic field H is shown in Fig. 65 together with the nomenclature used for the sub-levels. The transitions reported here are indicated.

* Work supported jointly by the Signal Corps and ONR.

† Submitted by Edward S. Dayhoff in partial fulfillment of requirements for the degree of Doctor of Philosophy in the Faculty of Pure Science, Columbia University.

‡ Present address: Central Radio Propagation Laboratory, Microwave Standards Section, National Bureau of Standards, Washington, D. C.

§ Present address: Watson Scientific Computing Laboratory, Columbia University, New York, New York.

¶ Present address: Department of Physics, Stanford University, Stanford, California.

¹²⁸ W. E. Lamb, Jr., and R. C. Retherford, Part I, Phys. Rev. **79**, 549 (1950); Part II, Phys. Rev. **81**, 222 (1951); Part III, Phys. Rev. **85**, 259 (1952); Part IV, Phys. Rev. **86**, 1014 (1952); Triebwasser, Dayhoff, and Lamb, Part V, Phys. Rev. **89**, 98 (1953). Frequent references to these papers are made. Chapters, sections, figures, equations, tables, appendices, and footnotes of Part VI are numbered consecutively after those of Parts I through V.

W. GENERAL PROGRAM

An inspection of the day to day variations of the results¹²⁹ obtained with the metastable beam electric resonance apparatus¹³⁰ prior to about a year ago suggested the possibility of systematic errors whose effect was judged to be somewhat less than 1 Mc/sec in the final result. On the other hand, the internal consistency of individual runs appeared to indicate a possible precision approaching 0.1 Mc/sec in the result. It thus appeared that a systematic attack on residual inadequacies in the procedure was in order. On the one hand, empirical corrections of observations were reduced in number and simplified in application; on the other, the experimental parameters of the measurement were determined in an improved manner.

96. Improvements

The chief empirical correction to be removed was the relatively uncertain one¹³¹ for "soft" component¹³² of the metastable beam which required a great deal of time consuming computation. New interaction spaces with essentially complete polarization of the rf¹³³ relieved the problem of overlapping resonances, since nearby resonances which might overlap the desired one usually require a different polarization. By this

¹²⁹ See Part IV, Sec. 84 and, in particular, Table XVI.

¹³⁰ Described in detail in Part II.

¹³¹ See Part IV, Sec. 73.

¹³² Atoms in β -state. See Part I, Sec. 16.

¹³³ Described in Part V, Sec. 87.